Effect of gadolinium inclusion on the raman spectra and photoluminescence of TiO_2 nanoparticles

J. Dhanalakshmi, D. Pathinettam Padiyan*

Department of Physics, Manonmaniam Sundaranar University, Tirunelveli, 627012, India

*Corresponding author, E-mail: dppadiyan@msuniv.ac.in; Tel: (+91) 9442063155

Received: 30 March 2016, Revised: 09 August 2016 and Accepted: 03 August 2016

DOI: 10.5185/amp.2016/215
www.vbripress.com/amp

Abstract

$Gd_xTi_{1-x}O_2$ nanocomposites with x=0.00, 0.02, 0.04, 0.06, 0.08 & 0.10 were prepared through sol-gel method. The samples were characterized using X-ray diffraction (XRD), diffuse reflectance spectroscopy (DRS), High resolution scanning electron microscope (HR-SEM), Raman spectroscopy and photoluminescence spectroscopy (PL). The XRD pattern and Raman spectra confirmed the presence of crystalline nature and phase pure anatase tetragonal system. The average crystallite size of the samples was between 10 to 18 nm. HR-SEM images indicated the formation of spherical like particles of $Gd_xTi_{1-x}O_2$ nanocomposites. An obvious reduction in particle size of $Gd_xTi_{1-x}O_2$ nanocomposites were noticed while comparing the SEM images of bare TiO_2 and composite samples. Coupling of Gd is responsible for slight blue shift in absorption edge. The presence of oxygen vacancies is confirmed in Raman and PL spectra. These oxygen vacancies potentially trap electrons and restrict the electron-hole recombination and thus improve the photocatalytic reactions.

Keywords: TiO_2, anatase, nanocomposites, raman, photoluminescence.

Introduction

The removal of organic compounds in waste water is a great deal of interest in the field of catalysis which utilizes the light energy and produces non-toxic by-products during the reaction. There are several semiconducting materials including ZnO, SnO_2, WO_3, Fe_2O_3 and TiO_2 have been widely investigated as photocatalysts. Among them, TiO_2 is advised as the most popular and promising photocatalyst due to its high stability, photo reactivity, chemical inertness, non-toxicity and low cost. It is a wide band gap semiconductor and used in various applications such as pigments, catalysts, energy storage, water splitting, dye-sensitized solar cells and sensors [**1-4**]. It exists in three crystalline phases namely anatase, rutile and brookite. Among them, anatase and rutile phases are mostly used in various applications. Brookite phase is not used in experimental investigations, because it is stable only at low temperatures. However, compared to rutile and brookite, anatase is the most active phase because of its adsorptive affinity towards organic compounds. Anatase phase plays a main role in dye decomposition and solar energy conversion due to its high photo activity [**5-8**]. But the wide band gap of TiO_2 responds light only from UV region which results in poor photocatalytic efficiency. Several efforts have been made to enhance the light absorbing ability of TiO_2. Coupled with metal oxides, non-metal oxides and inducing defect states in the TiO_2 lattice have been used to tune the optical energy band gap of TiO_2 [**9, 10, 11**]. Recently, it has been shown that coupling of lanthanides with TiO_2 matrix modify the electronic structure and optical properties of TiO_2, which improves the photocatalytic performance. The inclusion of rare earth ions can reduce the crystallite size and increase the surface area of TiO_2, which tends to restrict the electron-hole recombination and enhancement of adsorption capacity of TiO_2 for organic pollutants. It is reported that coupling of gadolinium would enhance the photocatalytic efficiency of TiO_2 due to the high adsorption capacity, half-filled electronic configuration, and the larger red shift [**12, 13**].

The properties of nanocomposites mainly depend on the preparation method. The nanocomposites of metal oxides are mainly prepared from co-precipitation, hydrothermal, solid state mixing, sol-gel methods, etc. Among these, sol-gel process is the most effective method for controlling the particle size, morphology and structural properties of the nanocomposites and produce homogeneous material with high surface area [**14, 15**].

In the present study, the $Gd_xTi_{1-x}O_2$ nanocomposites with x=0.00, 0.02, 0.04, 0.06, 0.08 and 0.10 are prepared by sol-gel method and the effect of inclusion of gadolinium on the structural, morphological and optical properties of the nanocomposites are investigated. Gadolinium is included in the TiO_2 matrix so as to decrease the particle size and to increase the surface area of these nanocomposites. Larger surface area of the nanocomposites will also provide larger number of active sites. This enhances the performance of photocatalytic degradation.

Experimental

Materials

Titanium (IV) isopropoxide (Purity-97%, Sigma Aldrich, India), Gadolinium (III) nitrate hexahydrate (Purity-99.9%, Sigma Aldrich, USA), ethanol and glacial acetic acid (purity-99 to 100% Merck, India) were purchased with analytical grade and used without purification. Double distilled (DD) water was used throughout the preparation method.

Preparation of $Gd_xTi_{1-x}O_2$ nanocomposites

$Gd_xTi_{1-x}O_2$ nanocomposites are prepared by sol-gel method using titanium isopropoxide ($Ti(OC_3H_7)_4$) as a precursor. 5 ml of titanium isopropoxide solution is added drop by drop with 5 ml of ethanol. Then 10 ml of double distilled water is added drop wise and the pH of the solution is adjusted to 3 by adding glacial acetic acid. After half an hour stirring, the resultant sol was allowed to gel for one day and then dried at 80 °C overnight. The resultant material is milled with mortar and pestle and annealed at 450 °C for 2 h to obtain TiO_2 (x=0.00). To prepare $Gd_{0.02}Ti_{0.98}O_2$ nanocomposites, 2 wt % of gadolinium nitrate (x=0.02) is added to the titanium isopropoxide solution and the same method of preparation is followed. Similarly, the inclusion of Gd content in the composition is varied as x=0.04, 0.06, 0.08 & 0.10.

Characterization

Powder X-ray diffraction (XRD) patterns are recorded from a PANalytical XPERT PRO X-ray diffractometer using Cu Kα radiation (λ=1.5405Å) at the scan rate of 0.05° per second. The optical properties are analyzed by UV-Vis diffuse reflectance (Shimadzu UV-2700) spectra measured in the wavelength range of 220-850 nm (with high-level absorbance measurements and a transmittance resolution of 0.000001 %). Raman spectra are obtained from Bruker RFS27 FT-Raman Spectrometer with an excitation wavelength of 1064 nm from Nd:YAG laser source. The surface morphology of nanocomposites is characterized using High Resolution Scanning Electron Microscope (FEI Quanta FEG 200HR-SEM). The luminescence property of the composites is studied using Cary Eclipse EL08083851 Fluorescence spectrometer with an excitation wavelength of 370 nm.

Results and discussion

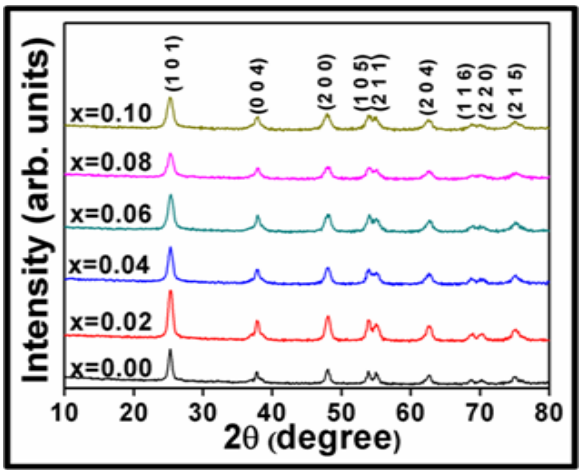

Fig. 1. XRD patterns of GdxTi1-xO2 nanocomposites.

The XRD patterns of $Gd_xTi_{1-x}O_2$ nanocomposites annealed at 450 °C are shown in **Fig. 1**. The XRD pattern confirms that all the prepared samples are purely in anatase phase. No characteristic peaks of gadolinium / gadolinium oxide are present. The diffraction peaks at 2θ values at 25.25°, 37.75°, 47.97°, 53.87°, 55.07°, 62.81°, 68.72°, 70.30° and 75.04° are indexed to (101), (004), (200), (105), (211), (204), (116), (220) and (215) planes of anatase TiO_2 respectively and matched with standard JCPDS no.: 84-1285. The lattice parameters are obtained from least squares procedure and shown in **Table. 1**.

Table. 1. XRD derived parameters for $Gd_xTi_{1-x}O_2$ nanocomposites.

	Unitcell parameters		
Sample	**a=b (Å)**	**c(Å)**	**Cell volume(Å)^3**
x=0.00	3.7843(2)	9.5152(5)	136.26(1)
x=0.02	3.7820(2)	9.5090(5)	136.35(1)
x=0.04	3.7800(2)	9.5255(6)	136.11(1)
x=0.06	3.7786(2)	9.4934(6)	135.55(1)
x=0.08	3.7958 (3)	9.4469(6)	136.11(2)
x=0.10	3.7912(3)	9.4723(6)	136.15(2)

It is evident that, as gadolinium inclusion increases, the (105), (211), (116) and (220) peaks in XRD patterns are suppressed. The decrease in X-ray intensity and the change in lattice parameters are observed on including Gd in the TiO_2 matrix. The change in lattice parameters a and c are due to the slight distortion in the crystal lattice of TiO_2. Due to large ionic radius of Gd (0.938 Å) it is impossible to enter into the substitutional position of Ti (0.64 Å) [**1, 4, 12**]. Hence, Gd has entered into the interstitial position of TiO_2 matrix. The average crystallite size is calculated using Scherrer's formula:

$$D = 0.9\lambda/\beta\, cos\theta, \qquad (1)$$

where λ is the wavelength of incident radiation, β is the full-width at half-maximum (FWHM) and θ is the Bragg angle. The average crystallite size is found to be in the range of 10 to 18 nm.

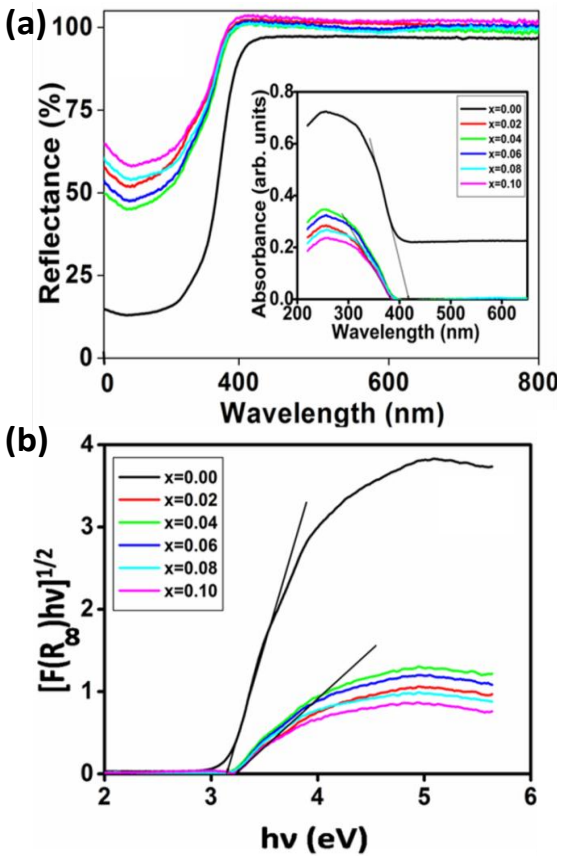

Fig. 2. (a) UV–vis diffuses reflectance spectrum of the samples. The inset shows its absorbance spectrum and (b) Kubelka-Munk graphs of $Gd_xTi_{1-x}O_2$ nanocomposites.

Fig. 2(a) shows the influence of gadolinium inclusion on the reflectance of TiO_2 nanoparticles which are measured at room temperature. The plot of $[F(R_\infty)\ h\nu]^{1/2}$ *vs* hν of $Gd_xTi_{1-x}O_2$ nanocomposites are shown in the **Fig. 2(b).** The band gap energy is calculated using Kubelka-Munk function.

$$K/S = F(R_\infty) = [2R_\infty / (1 - R_\infty)^2] \qquad (2)$$

where, K and S are the absorbance and scattering co-efficients respectively, $R_\infty = R_{sample}/R_{standard}$, $R_{standard}$ is the reflectance of the reference $BaSO_4$ and R_{sample} is the reflectance of nanocomposites. The optical band gap is determined by extrapolating the linear portion of $(F(R_\infty)h\upsilon)^{1/2}$ *vs* hυ plot to $F(R_\infty) = 0$ [**16, 17**] and the band gap values are between 3.151(2) to 3.235(1) eV. No considerable change in the band gap is observed due to the inclusion of Gd in TiO_2. The inset of **Fig. 2(a)** shows the absorption of $Gd_xTi_{1-x}O_2$ nanocomposites. The decrease in absorbance and the shift in absorbance towards shorter wavelength are attributed to the decrease in crystallite size of nanocomposites. The absorbance of TiO_2 observed at 415 nm corresponds to band gap 3.151(2) eV and the absorbance for $Gd_xTi_{1-x}O_2$ nanocomposites (x=0.10) occurred at 380 nm, which corresponds to band gap 3.235(1) eV. This leads to small increase in the band gap of the nanocomposites [**18, 19**].

The phase pure anatase nature of $Gd_xTi_{1-x}O_2$ nanocomposites are further confirmed using Raman spectra. The Raman peaks corresponding to anatase TiO_2 in both the pure TiO_2 and $Gd_xTi_{1-x}O_2$ nanocomposites are shown in **Fig. 3.** The Raman bands corresponding to the anatase phase appears at 144, 197, 396, 514, and 639 cm^{-1}. Any secondary Raman peaks related to Gd or its oxide phases are not detected which is well consistent with the XRD results.

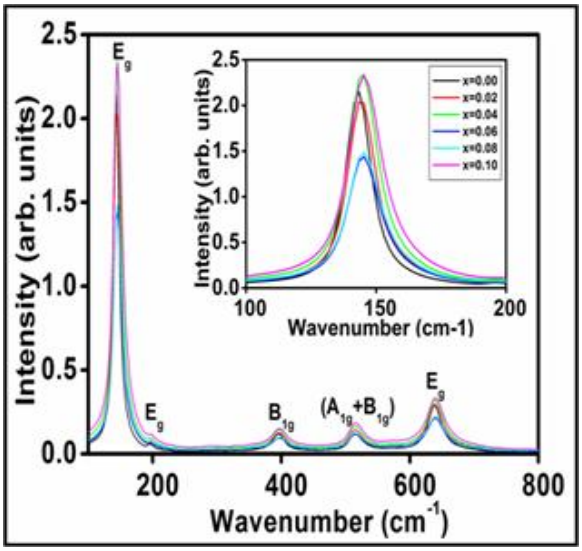

Fig. 3. FT-Raman spectra of $Gd_xTi_{1-x}O_2$ nanocomposites for various x value (The inset shows the shifting and broadening of the E_g mode).

The intense peak at 144 cm^{-1} corresponds to the E_g mode of anatase TiO_2. Other two low intense peaks of this mode appeared at 197 and 639 cm^{-1}, respectively. The B_{1g} mode at 396 cm^{-1} and the $(A_{1g} + B_{1g})$ mode appeared at 514 cm^{-1}. The E_g mode is due to the symmetric stretching vibration of O-Ti-O, the B_{1g} mode is associated with symmetric bending vibrations of O-Ti-O in TiO_2 and A_{1g} mode is the result of asymmetric bending vibration of O-Ti-O. As the inclusion of Gd increases, the position of the Raman bands in particular, the E_g mode at 144 cm^{-1} slightly shifts towards higher wavenumber side along with the peak broadening. Due to the mismatch of ionic radius of the Gd and Ti, gadolinium ion cannot enter into the smaller Ti lattice site and hence it has to occupy the interstitial position. This will introduce lattice distortion in the structure of TiO_2 and the charge difference between two metal ions produces the oxygen vacancies in the

TiO_2 lattice to maintain the charge neutrality. The other Raman peaks at 396, 514, and 639 cm^{-1} show variation in wavenumber due to distortion in the symmetry of O-Ti–O vibrations by the presence of increasing O-Gd–O vibrations. The presence of oxygen vacancies, lattice defects due to the displacement of oxide ions from their normal lattice positions leads to broadening and shifting of Raman active modes [**20-22**]. When the crystallite size decreases, the change in vibrational properties of nanocomposites occurs. Due to the size-induced radial pressure, a volume contraction occurs within the nanocomposites. The decrease in the interatomic distances leads to an increase in the force constants. The Raman peaks shift towards a higher wavenumber due to the increasing force constant [**23**].

Fig. 4 shows the HR-SEM images of $Gd_xTi_{1-x}O_2$ nanocomposites which reveals that it consists of spherical like particles. But the particle size of the nanocomposites is smaller than that of pure TiO_2. However, the inclusion of Gd leads to fuse the particles to form larger grains. As the Gd inclusion increases, the agglomeration of particles also increases. There are several voids present in the aggregation of nanoparticles. Low temperature annealing and low atomic diffusion leads to formation of voids in the surface of nanocomposites [**24**].

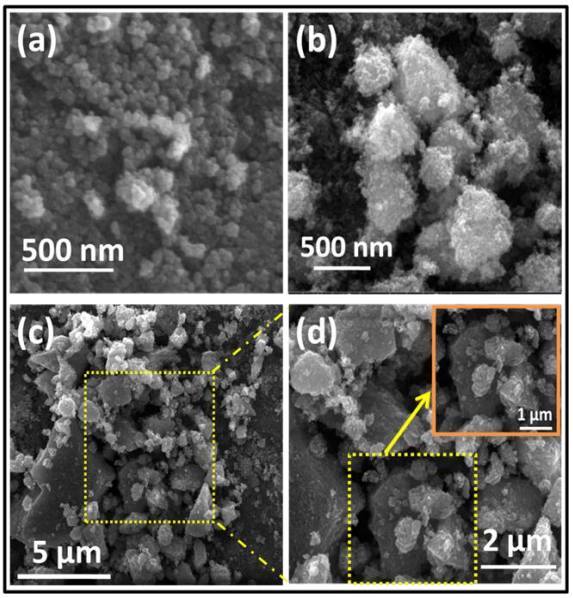

Fig. 4 HRSEM images of (a) pure, (b) x=0.02 and (c) & (d) x=0.10, $Gd_xTi_{1-x}O_2$ nanocomposites.

Photoluminescence emission spectrum is used to study the charge transfer behavior of the photo-generated electron-hole pairs and to understand the separation and recombination of photo-generated charge carriers. **Fig. 5** shows the PL spectra of $Gd_xTi_{1-x}O_2$ nanocomposites excited at 370 nm and all the emission peaks are in the visible region. Bare TiO_2 shows near band edge emission peak at 420 nm whereas for nanocomposites at 428 nm. The intensity of this emission peak is suppressed with the incorporation of Gadolinium. The peaks of PL spectra of $Gd_xTi_{1-x}O_2$ composites show lesser intensity and are shifted towards the lower band gap region (from 531 nm to 524 nm) when compared to bare TiO_2. The violet emission at 428 nm (2.89 eV), blue emission at 469 nm (2.64 eV) and green emission at 524 nm (2.36 eV) are attributed to band-edge free excitons and bound excitons. The emission at 428 nm is attributed to self-trapped excitons (STE) located at TiO_6 octahedra arising due to interaction of conduction band electrons localized on the Ti 3d orbital with holes present in the O 2p orbital of TiO_2, while the emission peaks at 469 and 524 nm are ascribed to oxygen vacancy related trap states. It is due to the oxygen vacancies associated with Ti^{3+} in anatase TiO_2. The F-centre is formed because of the trapping of electron pair in the vacant cavity due to the loss of an O atom in the TiO_2 lattice. Ti^{3+} and F^+ centres arise within the band gap of the material due to occupation of one electron in the F-centre in neighboring Ti^{4+} ion. These centers are called as F (two electrons), F^+ (one electron) and F^{2+} (devoid of electrons) depending on the number of trapped electrons. **Fig. 6** shows the formation of STE and F-centre. The variation in the PL emission intensity is due to the formation of different defect states in the band gap of TiO_2. In the photoluminescence process, the negatively charged electrons in the conduction band are captured by the oxygen vacancies through a non-radiative process and recombines with the positively charged photogenerated holes in the valence band along with fluorescence emission [**25-29**].

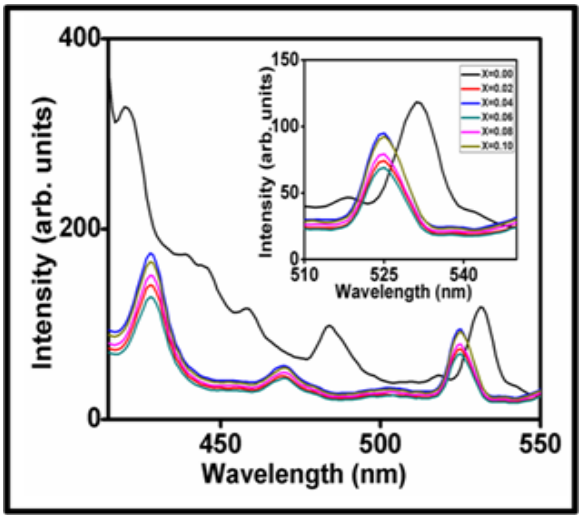

Fig. 5 Photoluminescence spectra of $Gd_xTi_{1-x}O_2$ nanocomposites. The inset shows shifting of 531 nm peak towards lower wavelength.

Inclusion of gadolinium improves the oxygen vacancies on the surface of the GdxTi1-xO2 nanocomposites. The separation of photo generated electron-hole pairs is must for obtaining good photocatalytic performance. The electrons are

confined in the oxygen vacancies. Therefore, the electrons are not easily available to undergo radiative recombination with holes.

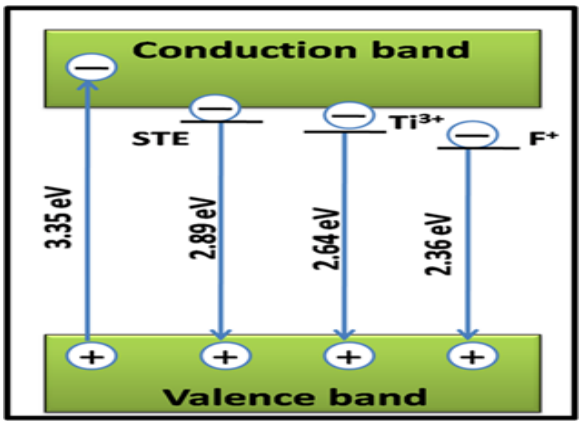

Fig. 6. Excitation and emission wavelength (corresponding band gap) of PL spectra.

The oxygen vacancies extend the lifetime of charge carriers and enhance the photocatalytic activity by promoting the charge separation of negatively charged electrons and positively charged holes. These charge carriers contribute in enhancing the photocatalytic degradation of dyes under visible light irradiation. Oxygen vacancies present in the nanocomposites act as active centers for electron trap centers which improve the photocatalytic activity of the nanocomposites [**30**]. When illuminating the sample with UV/Vis light the electrons are excited to the conduction band and holes are created in the valence band. During this process, few electrons move towards the conduction band while few others are trapped in the levels created due to Gd 4f state. These trapped electrons easily react with the atmospheric O_2 molecules to convert it to superoxide radicals. These superoxide radicals act as a potential candidate in the photocatalysis process.

Conclusion

$Gd_xTi_{1-x}O_2$ nanocomposites with x=0 to 0.1 were successfully synthesized using sol-gel method. XRD studies confirmed the anatase phase of $Gd_xTi_{1-x}O_2$ nanocomposites. The average crystallite size of all the samples was found to be 10 to 16 nm. The effect of inclusion of Gd is confirmed from the shifting and broadening of Raman bands. The peaks observed in the visible region of PL spectra are due to the defect levels created by oxygen vacancies. $Gd_xTi_{1-x}O_2$ nanocomposites will act as better photocatalyst than pure TiO_2 nanoparticles, due to its smaller particle size, crystallite size and increase in vacancy defects. The increase in oxygen vacancies will provoke charge separation which reduces the rate of recombination of electron-hole pairs.

Acknowledgements

One of the authors, J. Dhanalakshmi gratefully acknowledges the University Grant Commission (UGC), New Delhi for UGC-BSR fellowship in performing the present research work. The authors thank SAIF, IIT Madras for recording FT-Raman spectra and Department of Physics, Alagappa University for recording PL spectra.

References

1. Farbod, M.; vala, M.K.; *Powder Technol*. **2013**, *239*, 434.
2. Kumar, A.; Madaria, A.R.; Zhou, C; *J. Phys. Chem*. C., **2010**, *114*, 7787.
3. Lee, D.Y.; Lee, M.H.; Cho, N.I; *Curr. Appl. Phys*. **2012**, *12*, 1229.
4. Paul, S.; Chetri, P.; Choudhury, B.; Ahmed, G.A.; Choudhury, A; *J. Colloid Interface Sci.*, **2015**, *439*, 54.
5. Reyes-Coronado, D.; Rodriguez-Gattorno, G.; Espinosa Pesqueira, M. E.; Cab, C.; de Coss, R.; Oskam, G; *Nanotechnology*. **2008**, *19*, 145605.
6. Zhang, J.; Zhou, P.; Liu, J.; Yu, J; *Phys.Chem.Chem.Phys.* **2014**, *16*, 20382.
7. Yang, Z.; Wang, B.; Cui, H.; An, H.; Pan, Y.; Zhai, J; *J. Phys. Chem. C.*, **2015**, *119*, 16905.
8. Singh, S.; D'Britto, V.; Bharde, A.; Sastry, M.; Dhawan, A.; Prasad, B. L.V; *Int. J. Green Nanotechnol.*, **2010**, *2*, 80.
9. Kumar, S.G.; Devi, L.G.; *J. Phys. Chem. A.*, **2011**, *115*, 13211.
10. Pan, X.; Yang, M.Q.; Fu, X.; Zhang, N.; Xu, Y.J; *Nanoscale*, **2013**, *5*, 3601.
11. Hernandez-Ramırez, A.; Medina-Ramırez, I. (Eds.); Photocatalytic Semiconductors: Synthesis, Characterization, and Environmental Applications; Springer: Switzerland, **2015**.
12. Sudhagar, P.; Devadoss, A.; Nakata, K.; Terashima, C.; Fujishima, A.J.; *Electrochem.Soc.* **2015**, 162, 3.
13. Liu, H.; Liu, G.; Xie, G.; Zhang, M.; Hou, Z.; He, Z; *Appl. Surf. Sci*., **2011**, *257*, 3728.
14. Binitha, N.N.; Yaakob, Z.; Resmi, R; *Cent. Eur. J. Chem*. **2010**, *8*, 182.
15. Ismail, A.A.; Ibrahim, I.A.; *Appl.Catal., A*., **2008**, 346, 200.
16. Yang, L.; Kruse, B; *J. Opt. Soc. Am. A*., **2004**, *21*, 1933.
17. Wood, B. J.; Strens, R. G. J. *Mineral Mag*., **1979**, *43*, 509.
18. Liqiang, J.; Xiaojun, S.; Baifu, X.; Baiqi, W.; Weimin, C.; Honggang, F; *J. Solid State Chem*., **2004**, *177*, 3375.
19. Gschneidner, K.A.; Bünzli, J.C.G;. Pecharsky, V.K. (Eds.); Handbook on the Physics and Chemistry of the rare earths optical spectroscopy, Elsevier: North-Holland, **2007**.
20. Ohsaka, T.; Izumi, F.; Fujiki, Y; *J. Raman Spectrosc*., **1978**, *7*, 321.
21. Ohsaka, T; *J. Phys. Soc. Jpn*. **1980**, *48*, 1661.
22. Tian, F; Zhang, Y; Zhang, J; Pan, C; *J. Phys. Chem. C*, **2012**, *116*, 7515.
23. Pal, M.; Pal, U.; Jimenez, J.M.G.Y.; Perez-Rodriguez, F; *Nanoscale Res. Lett*., **2012**, *7*, 1.
24. Choudhury, B.; Dey, M.; Choudhury, A; *Int. Nano Lett*., **2013**, *3*, 25.
25. Hashmi, M. S. J. (Eds.); Comprehensive Materials Processing, Elsevier: Italy, **2014**.
26. Zhang, W.F.; Zhang, M.S.; Yin, Z.; Chen, Q; *Appl. Phys. B*., **2000**, *70*, 261.
27. Song, S.; Sheng, Z.; Liu, Y.; Wang, H.; Wu, Z; *J. Environ. Sci*., **2012**, *8*, 1519.
28. Tripathi, A.K.; Mathpal, M.C.; Kumar, P.; Agrahari, V.; Singh, M.K.; Sheo Kumar Mishra; Ahmad, M. M.; Arvind A; *Adv. Mater. Lett*., **2015**, *3*, 201.
29. Lei, Y.; Zhang, L.D; *J. Mater. Res*., **2001**, *4*, 1138.
30. Islam, M.J.; Reddy, D.A.; Choi, J.; Kim, T.K.; *RSC Adv.* **2016**, *6*, 19341.

